

## Redistribution of La-Al nearest-neighbor distances in the metallic glass $\text{Al}_{0.91}\text{La}_{0.09}$

A. Frenkel and E. A. Stern

*Department of Physics, Box 351560, University of Washington, Seattle, Washington 98195*

A. Voronel, A. Rubshtein, Y. Ben-Ezra, and V. Fleurov

*School of Physics and Astronomy, R. and B. Sackler Faculty of Exact Sciences, Tel Aviv University, Ramat Aviv 69978, Israel*

(Received 24 January 1996)

X-ray-absorption fine-structure (XAFS) measurements of metallic glass  $\text{Al}_{0.91}\text{La}_{0.09}$  and a crystalline phase  $\text{Al}_{11}\text{La}_3$  formed by annealing of the glass were made at the La  $L_3$  edge and analyzed by the splice method. The first-neighbor partial radial distribution functions about the La atoms for the crystal and glass were obtained at  $T=12$  K demonstrating the difference between their local structures. The shortest La-Al distance (mean value  $3.09 \pm 0.05$  Å) within the glass was distinctively smaller than within the crystal  $\text{Al}_{11}\text{La}_3$  ( $3.21 \pm 0.05$  Å). This partial shortening of the La-Al bonds decreases the size mismatch between the La and Al atoms making the glass formation more favorable with anomalously low content of La during the quench. Monte Carlo simulations were performed for the Al-La glass and agreement with the XAFS result was obtained. [S0163-1829(96)08826-1]

### I. INTRODUCTION

Amorphous alloys with anomalously high content of Al (higher than 90%), e.g., binary alloys Al-Ln (lanthanide metal) and ternary alloys  $\text{Al}_{0.91}\text{La}_{0.05}\text{Ni}_{0.04}$ ,  $\text{Al}_{0.91}\text{Ce}_{0.05}\text{Ni}_{0.04}$  and others were recently synthesized.<sup>1,2</sup> These amorphous alloys are ductile and have tremendous strength and high corrosion resistance as well as low density. Such a small concentration of lanthanide in an amorphous phase seems rather unexpected and has no analogy in the literature.<sup>3</sup> The present work examines the structure of the amorphous alloy  $\text{Al}_{0.91}\text{La}_{0.09}$  for better understanding of the reason for these unexpected properties.

We used both x-ray diffraction to characterize the samples and the x-ray-absorption fine-structure (XAFS) method to probe the local atomic environment. The advantage of XAFS over many other techniques is its ability to select a specific element as a central atom and to study the radial distribution of its nearest neighbors. XAFS allows us also to perform a comparative analysis of an *unknown* structure by checking the results against some known (*standard*) material so as to quantitatively determine the accuracy of the analysis technique. Thus the investigation of both the amorphous alloy  $\text{Al}_{0.91}\text{La}_{0.09}$  and the crystalline phase  $\text{Al}_{11}\text{La}_3$  which nucleates from the glass when annealed<sup>4</sup> is an excellent case fitting this scheme. The ordered crystalline phase serves as a *standard* for calibrating the accuracy of the determination of the structure of the *unknown* glassy phase.

The present paper applies the splice method of XAFS to metallic glasses. The splice method, described elsewhere,<sup>5</sup> has been previously demonstrated in the analysis of the systems with known structure like aperiodic crystals Mn-Al-Si and biological proteins.<sup>5</sup> It has important advantages over other methods of XAFS analysis (fitting technique or ratio method<sup>6</sup>) if the *unknown* structure has a distribution which differs strongly from a Gaussian disorder and only one atom type is involved as the first neighbor, as occurs in the case here.

We tested the splice method first against the known structure ( $\text{Al}_{11}\text{La}_3$ ) determined by diffraction to check the reliability of the method. The XAFS data are missing the low  $k$  (photoelectron wave number) information which has to be reconstituted from cumulants obtained by the ratio method to derive the radial distribution functions (RDF's) of the first neighbors to the La atoms for crystal and glass. The crystal RDF was then compared with the calculated RDF constructed from the known interatomic distances and their mean-squared deviations (Debye-Waller factors) determined by diffraction measurements of the crystal structure and fits to the XAFS data, respectively.

The RDF's are the partial pair-distribution functions around the La atoms in both the crystal and the glass. While the centroids of RDF's of Al neighbors to La for both crystal and glass are close to each other, the details of the distributions are different. The glassy structure is shown to be more compact and the corresponding distribution more symmetric than that in the crystal. While frequently the local structures of the glass and the corresponding crystal are similar, the glass in this case looks completely different from the crystalline phase. The fraction of nearest-neighbor La-Al pairs has bond length smaller than in the crystalline phase. This partial shortening of bonds, mainly due to the decrease of the larger La atom radius, is favorable for their alloying in a single phase, thus explaining their glass formation with anomalously low concentration of La.

An outline of the paper is as follows. Section II contains the theoretical background of the splice method. Sample preparation and XAFS measurements are described in Sec. III. Data analysis and results are given in Sec. IV, Monte Carlo simulations are described in Sec. V, discussion is given in Sec. VI, and summary and conclusions are presented in Sec. VII.

### II. FORMALISM

Following Refs. 5–9 we assume that the XAFS  $\chi(k)$  of an isolated shell with  $N$  atoms of one type may be written

$$\chi(k) = B(k) \int_0^\infty e^{i2kr'} g(r') dr', \quad (1)$$

where

$$B(k) = \frac{t(2k)}{k} \frac{mS_0^2}{4\pi\hbar^2} e^{i\delta(k)}, \quad g(r') = \frac{\rho(r')}{r'^2} e^{-2r'/\lambda}. \quad (2)$$

Here  $t(2k)$  and  $\delta(k)$  are the effective backscattering amplitude and phase of the atom in the shell,  $k = (1/\hbar)\sqrt{2m(E-E_0)}$  is the photoelectron wave number,  $E$  is the photon energy, and  $E_0$  is the zero of the muffin-tin potential.  $S_0^2$  is the passive electron reduction factor,<sup>7</sup>  $\lambda$  is the mean free path of the photoelectron.  $\rho(r')$  is the RDF, obeying the following normalization condition:  $\int_0^\infty \rho(r') dr' = N$ , the coordination number.

Assume that we have  $\chi_s(k)$  of some *standard* structure with known effective distribution  $g_s(r)$  which in the case of small deviation from Gaussian may be presented by a cumulant expansion:<sup>7</sup>

$$\int e^{i2k\Delta r} g_s(r) dr = \exp \sum_{n=0}^{\infty} \frac{(2ik)^n}{n!} C_n, \quad (3)$$

where  $\Delta r = r - r_s$ ,  $r_s$  is the centroid of  $g_s(r)$  and  $C_0 = \ln(\int_0^\infty g_s(r) dr)$ . The next four leading cumulants of Eq. (3) are related to the power moments  $p_n$  of  $g_s(r)$ :

$$C_1 = p_1 = 0, \quad C_2 = p_2, \quad C_3 = p_3, \quad C_4 = p_4 - 3p_2^2,$$

$$p^n \equiv \langle (r - r_s)^n \rangle_{g_s} = \frac{\int (r - r_s)^n g_s(r) dr}{\int g_s(r) dr}. \quad (4)$$

Using the ratio method of XAFS data analysis<sup>6,7,9</sup> one can eliminate the  $B(k)$  of the *unknown* by dividing  $\chi_u(k)$  of the *unknown* by a *standard*  $\chi_s(k)$ , where

$$\chi_s(k) = N_s \frac{B(k)}{r_s^2} e^{i2kr_s} e^{-2k^2\sigma_s^2} e^{-2r_s/\lambda}. \quad (5)$$

Here  $N_s$  and  $\sigma_s^2$  are the coordination number and the second cumulant (Debye-Waller factor) of the *standard*. At this point we assume that the distribution  $g_s(r)$  is Gaussian. Equation (5) is valid only if the *unknown* and the *standard* have similar chemical environment around La atoms, and, therefore,  $B(k)$  are the same in their XAFS signals,  $\chi_u(k)$  and  $\chi_s(k)$ .

Let us consider for simplicity the *standard* structure containing only 1 atom in the shell by setting  $N_s = 1$  and  $\sigma_s^2 = 0$ . Dividing  $\chi_u(k)$  by  $\chi_s(k)$ , we obtain  $\chi'(k)$ :

$$\chi'(k) = r_s^2 e^{-i2kr_s} \int_0^\infty \frac{\rho(r')}{r'^2} e^{i2kr'} e^{-2(r'-r_s)/\lambda} dr'. \quad (6)$$

If the *standard* has been chosen properly,  $r - r_s \ll \lambda$ . Thus  $e^{-2(r'-r_s)/\lambda} \approx 1$ , to a good approximation. Using the identity

$$\chi'(k) e^{i2kr_s} = |\chi'(k)| \exp\{i[2kr_s + \Delta\Psi(k)]\}, \quad (7)$$

$$\Delta\Psi(k) = \arg\chi_u(k) - \arg\chi_s(k),$$

one can now convert Eq. (6) and take an imaginary part:

$$\frac{|\chi'(k)|}{r_s^2} \sin[2kr_s + \Delta\Psi(k)] = \int_0^\infty \sin(2kr') \frac{\rho(r')}{r'^2} dr'. \quad (8)$$

Applying the  $\sin(2kr)$  transform to the both parts of Eq. (8) we obtain the RDF:

$$\rho(r) = \frac{4}{\pi} \frac{r^2}{r_s^2} \int_0^\infty |\chi'(k)| \sin[2kr_s + \Delta\Psi(k)] \sin(2kr) dk. \quad (9)$$

To calculate the integral in Eq. (9) one must take into account that  $\chi'(k)$  is measured within the finite  $k$  range, between  $k_1$  and  $k_2$ . In order to extrapolate  $\chi'(k)$  to the low- $k$  range between  $k_1$  and 0, one treats the effective distribution  $g(r)$  at low  $k$  by a cumulant expansion  $\{C_i\}$  to the third order, following Ref. 5:

$$\ln|\chi'(k)| = \ln\left[r_s^2 \int_0^\infty g(r') dr'\right] - 2k^2 C_2,$$

$$\arg\chi'(k) = \Delta\Psi(k) = 2k C_1 - \frac{4}{3} k^3 C_3. \quad (10)$$

Note that  $C_1 = \langle r - r_s \rangle_g \neq 0$  since  $r_s$  is a centroid of  $g_s(r)$  rather than  $g(r)$ . To reduce the cutoff wiggles from the upper limit of the data range,  $k_2$ , we multiply the integrand in Eq. (9) by the Gaussian cutoff factor  $\exp(-2k^2\sigma_c^2)$  such that  $\exp(-2k_2^2\sigma_c^2) \ll 1$ . The spatial resolution introduced by this cutoff factor is given by  $\delta r = 2.5\sigma_c$ . If no cutoff factor is used, the spatial resolution is determined as

$$\delta r = \frac{1}{2k_2}. \quad (11)$$

Finally, we ‘‘splice’’ the two ratios,  $\chi'(k)$ , one measured between  $k_1$  and  $k_2$ , and another one, extrapolated with cumulants between 0 and  $k_1$ , to evaluate the RDF [Eq. (9)]. We applied this method to the analysis of both the metallic glass  $\text{Al}_{0.91}\text{La}_{0.09}$  and the crystalline phase  $\text{Al}_{11}\text{La}_3$ .

### III. SAMPLE PREPARATION AND EXPERIMENT

Amorphous ribbons (40  $\mu\text{m}$  thick) of metallic glass  $\text{Al}_{0.91}\text{La}_{0.09}$  were produced by melt spinning in the Technion (Haifa, Israel).<sup>2</sup> The rapidly quenched alloys (the estimated quenching rate was  $5 \times 10^5$  K/sec) were produced in vacuum. The melt was heated to the predetermined temperature (1373 K) in an alumina crucible placed in a furnace. The glassy nature of the samples was verified by x-ray diffraction. The composition was tested by an electron microprobe.

To avoid the sample thickness effect in XAFS,<sup>10</sup> the glassy ribbon was thinned by rolling to the optimal thickness 20  $\mu\text{m}$ , satisfying the condition  $\Delta\mu x \ll 1$ , where  $x$  is the sample thickness and  $\Delta\mu$  is the absorption  $L_3$  edge step. The crystalline phase  $\text{Al}_{11}\text{La}_3$  was then obtained by annealing some of the ribbons in an evacuated and sealed quartz tube for 5 h at  $T = 510$   $^\circ\text{C}$ , well above the glass transition temperature. The crystallization in the ribbons was verified by x-ray-diffraction measurements which showed sharp Bragg peaks of both pure Al and  $\text{Al}_{11}\text{La}_3$  phases. The XAFS measurements on the La  $L_3$  edge (photon energy is 5483 eV) were performed on the beamline X11A at NSLS using a double crystal (111) Si monochromator. The data range (400

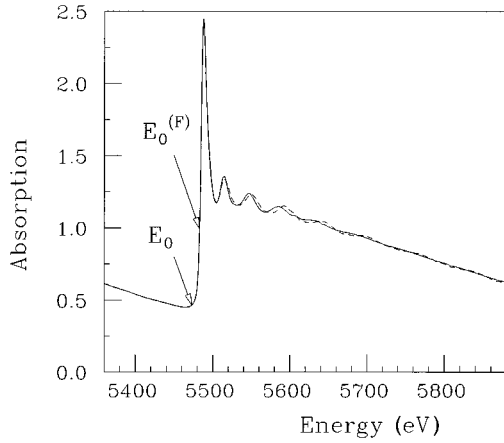


FIG. 1. Energy reference points  $E_0$  and  $E_0^{(F)}$  on the absorption curves of the glass (solid) and crystal (dash).

eV past the  $L_3$  edge) was limited by the  $L_2$  edge (5891 eV). The low-temperature measurements were taken using a Displex refrigerator.

#### IV. DATA ANALYSIS AND RESULTS

XAFS function  $\chi(k)$  is given by

$$\chi(k) = \frac{\mu(k) - \mu_0(k)}{\Delta\mu(0)}, \quad (12)$$

where  $\Delta\mu(0)$  is the  $L_3$ -edge jump on the absorption curve  $\mu(k)$ , and  $\mu_0(k)$  is a smooth atomic background. To remove the background from the data, the AUTOBK code<sup>11</sup> was used for both the glass and crystal data.

Special care was taken to determine correctly the  $k=0$  point. The absorption edge energy for metals is given by  $E_{\text{mt}} + E_f$ , where  $E_{\text{mt}}$  is the zero of potential of the interstitial region obtained in the muffin-tin approximation.<sup>12</sup>  $E_f$  is the Fermi energy (relative to  $E_{\text{mt}}$ ), usually taken somewhere on the edge. This definition of the absorption edge energy is elaborated in computer code FEFF5,<sup>12</sup> which constructs theoretical  $\chi(k)$  for a model structure, and will be referred to as  $E_0^{(F)}$ . For our purpose, however, so defined  $E_0^{(F)}$  is a poor reference point for the photoelectron wave number  $k$ . Indeed, in accordance with the Pauli principle the transition occurs to the first unoccupied level and the lowest possible wave number for a metal is  $k_f = (1/\hbar)\sqrt{2mE_f} = \sqrt{0.263E_f}$ , where the units of  $k$  and  $E$  are  $\text{\AA}^{-1}$  and eV, respectively. Therefore, to achieve the true  $k=0$  limit of the integral in Eq. (9) one must set  $E_0 = E_{\text{mt}} = E_0^{(F)} - E_f$ . In many materials it is a good initial approximation to choose the Fermi energy position at half maximum of the edge jump. If the structural

TABLE I. Parameters of background subtraction  $k_{\text{min}}$ ,  $k_{\text{max}}$  are the limits of the data range in  $k$  space,  $k^w$  is the weighting parameter,  $\delta k$  are the Hanning window margins,  $E_0$  and  $E_0^{(F)}$  for crystal  $\text{Al}_{11}\text{La}_3$  and glass  $\text{Al}_{0.91}\text{La}_{0.09}$ .

$k_{\text{min}}$ ( $\text{\AA}^{-1}$ )	$k_{\text{max}}$ ( $\text{\AA}^{-1}$ )	$k^w$	$\delta k$ ( $\text{\AA}^{-1}$ )	$E_0$ (eV)	$E_0^{(F)}$ (eV)
2.57	10.45	2	0.05	5473	5483

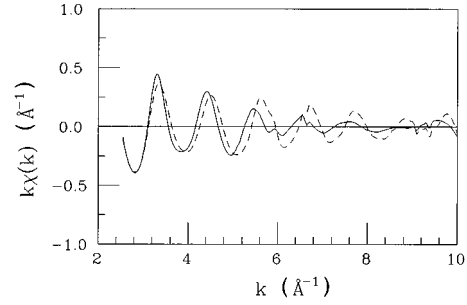


FIG. 2.  $\chi(k)$  (weighted with  $k$ ) of the glass (solid) and crystal (dash).

model is available, one can use theory (e.g., FEFF5) to correct this approximation by  $\Delta E_0$ , found from fit of theory to data. In our case, we first picked a point at 5482 eV (half maximum of the edge jump) as a first approximation and then shifted it forward by  $\Delta E = 1.0$  eV, as determined with 0.5 eV uncertainty from the fit of FEFF5 theory to the reference crystalline structure  $\text{Al}_{11}\text{La}_3$  as described below. Finally, we lowered the obtained value of the Fermi energy (5483 eV) by  $E_f$  to obtain the muffin-tin energy  $E_{\text{mt}}$ . The values of  $k_f$  and  $E_f$  are provided by FEFF5 for a given central atom. For the central atom La the values calculated by FEFF5 are  $k_f = 1.596 \text{\AA}^{-1}$ ,  $E_f = 9.7$  eV. These two different reference points,  $E_0$  and  $E_0^{(F)}$ , are shown in Fig. 1 for La  $L_3$ -edge absorption curves of  $\text{Al}_{11}\text{La}_3$  and  $\text{Al}_{0.91}\text{La}_{0.09}$ . Since a typical difference in Fermi energies between the standard and unknown materials could not be more than 1–2 eV, we set the same  $E_0^{(F)}$  for both materials. This leads to the 2% uncertainty in the determination of  $k_1$  of the glass. Parameters of the background subtraction,  $k_{\text{min}}$ ,  $k_{\text{max}}$  (the limits of the data range in  $k$  space),  $k^w$  (weighting parameter),  $\delta k$  (Hanning window margins),  $E_0$  and  $E_0^{(F)}$  are given in Table I for both the glass and crystal data. Figure 2 shows the  $\chi(k)$  obtained for the glass and crystal data by the above procedure.

To check the accuracy of the splice method the XAFS data of the crystal  $\text{Al}_{11}\text{La}_3$  were analyzed first.  $\text{Al}_{11}\text{La}_3$  belongs to the  $Immm$  space group (body-centered orthorhombic),<sup>13</sup> the elementary cell is shown in Fig. 3. At the first step, the fitting technique was used to resolve the structure around the La atom. At 12 K the zero-point vibration is the only contribution to the disorder in atomic posi-

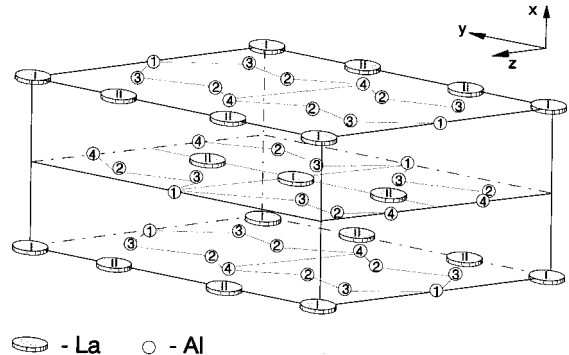


FIG. 3. Elementary cell of  $\text{Al}_{11}\text{La}_3$ . Numbers in circles correspond to inequivalent sites of Al and La atoms (see also Table II).

TABLE II. Coordination numbers  $N_i$ , fraction coefficients  $\nu_i$ , pair lengths of La-Al pairs:  $r_i^{(300)}$  at  $T=300$  K (Ref. 13) and  $r_i^{(12)}$  at 12 K (this work, using the same contraction coefficient  $\alpha=(1.35\pm 0.20)\times 10^{-2}$  for all pairs as defined by XAFS) for  $\text{Al}_{11}\text{La}_3$ . Uncertainties are shown in parentheses.

Pair	$N_i$	$\nu_i$	$r_i^{(300)}$ (Å)	$r_i^{(12)}$ (Å)
La(2)-Al(3)	4	2/3	3.249	3.21(1)
La(2)-Al(2)	4	2/3	3.257	3.21(1)
La(2)-Al(4)	2	2/3	3.267	3.22(1)
La(2)-Al(1)	2	2/3	3.271	3.23(1)
La(1)-Al(3)	4	1/3	3.305	3.26(1)
La(1)-Al(2)	8	1/3	3.385	3.34(1)
La(1)-Al(4)	4	1/3	3.615	3.57(1)
La(2)-Al(3)	2	2/3	3.631	3.58(1)
La(2)-Al(2)	2	2/3	3.738	3.69(1)

tions. The vibrational amplitude at this temperature may be safely approximated by the second cumulant only.

As one can see from Table II, there are two inequivalent sites of La atoms in the cell, La(1) and La(2). The total XAFS signal therefore, is a combination of the two signals:

$$\chi_{\text{La}}(k) = \frac{1}{3}\chi_{\text{La(1)}}(k) + \frac{2}{3}\chi_{\text{La(2)}}(k), \quad (13)$$

where coefficients  $\frac{1}{3}$  and  $\frac{2}{3}$  account for the different occupancy of atoms La(1) and La(2) in the cell. Table II shows that each site has 16 Al nearest neighbors which are distributed over nine different distances. The difference in the distances varies within 0.01–0.2 Å. The next coordination shell, populated by La atoms, is well separated from the farthest La-Al nearest-neighbor distance by  $\approx 0.4$  Å.

The crystal distances, measured at room temperature, were taken from Ref. 13. The fit of the theoretical  $\chi(k)$  to the crystal data was performed in  $r$  space within the range 2.0–4.3 Å using the program FEFFIT.<sup>14</sup> The fit parameters were  $S_0^2$ , contraction coefficient  $\alpha=(r^{(300)}-r^{(12)})/r^{(12)}$ , used to find distances  $r^{(12)}$  at 12 K by correcting for thermal contraction of room temperature distances  $r^{(300)}$ , and assumed to be the same for all distances, the shift of the energy origin  $\Delta E_0$ , and two Debye-Waller factors,  $\sigma_{\text{La-Al}}^2$  for all La-Al bonds and  $\sigma_{\text{La-La}}^2$  for La-La bonds. The fit result is shown in Fig. 4(a) over the region between the arrows.  $S_0^2$  was found to be  $0.95\pm 0.05$ . Thermal contraction  $\alpha=(1.35\pm 0.20)\times 10^{-2}$ , found from the fit, was used to find the distances  $r_i^{(12)}$  at 12 K (Table II). The small Debye-Waller factors ( $\sigma_{\text{La-Al}}^2=0.0027$  Å<sup>2</sup>,  $\sigma_{\text{La-La}}^2=0.0035$  Å<sup>2</sup>) of vibrations justified the Gaussian approximation made above.

Since all the Al atoms are situated almost at the same distance from the central La atom and their chemical environment is similar, the backscattering amplitude and phase shift can be approximated by the average distance  $r_s=3.3$  Å at temperature 12 K. Figure 5 shows that this approximation is valid since the  $k$  dependence of the scattering amplitude remains almost the same for all different paths to Al atoms for  $k>3$  Å<sup>-1</sup> (the region utilized from the XAFS

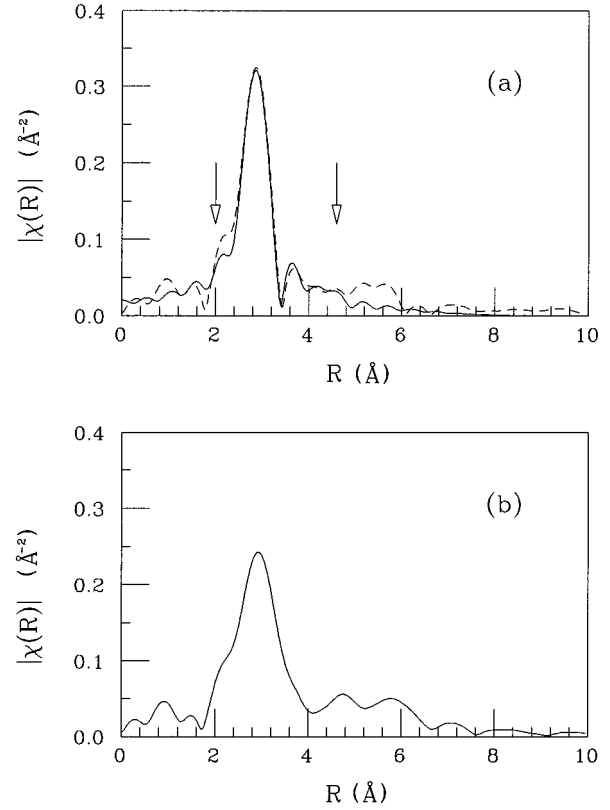


FIG. 4. (a) Fit to the  $\text{Al}_{11}\text{La}_3$   $|\chi(r)|$ : dash is for data, solid is for theory. The fitting range is shown by arrows. (b)  $|\chi(r)|$  of  $\text{Al}_{0.91}\text{La}_{0.09}$  glass.

data) and therefore can be reliably represented by the amplitude of the effective path we just defined.

To isolate the first shell the  $r$  range from 2.0 to 4.0 Å was chosen. The range was limited from the higher  $r$  so as not to include the more distant La neighbors in the crystal. The unknown crystal data  $\chi_u(r)$  and the standard  $\chi_s(r)$  were then back Fourier transformed to  $k$  space and their ratio  $\chi'(k)$  was obtained. The cumulants at low  $k$  were determined by fit to Eq. (10) within the  $k$  range 3–4 Å<sup>-1</sup>. The

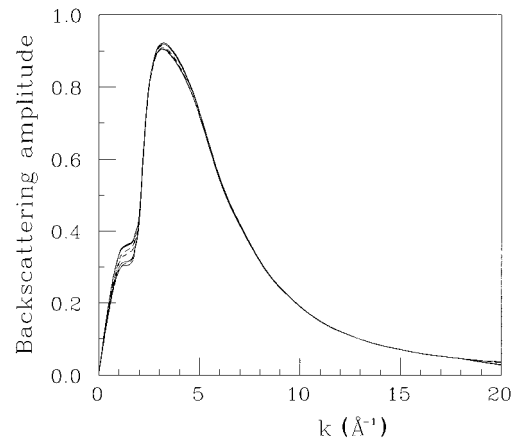


FIG. 5. Backscattering amplitudes  $t(k)$  calculated with FEFF5 for the paths La(1)-Al (dashes) and La(2)-Al (solid). All the paths are single-scattering paths from central atoms to their first-nearest neighbors in  $\text{Al}_{11}\text{La}_3$ .

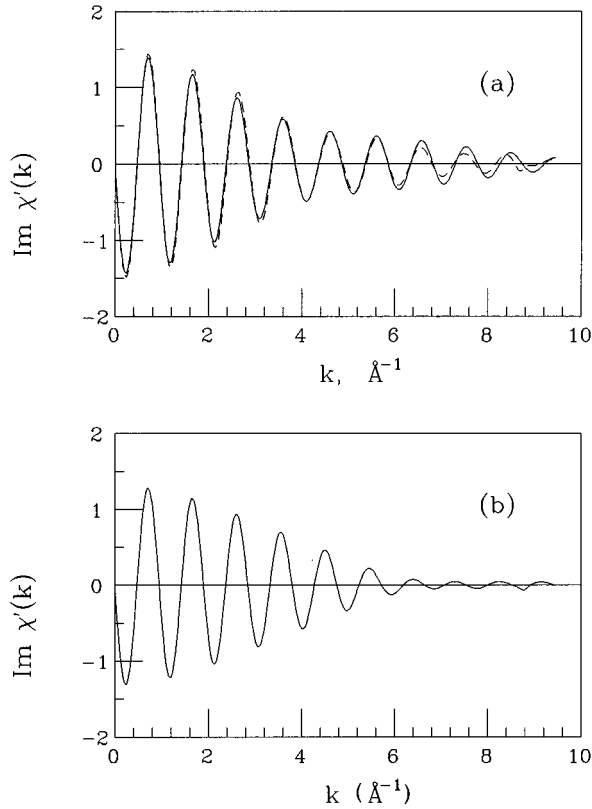


FIG. 6.  $\text{Im } \chi'(k)$  (multiplied by cutoff factor) of (a) crystal  $\text{Al}_{11}\text{La}_3$  (from XAFS data shown by dash, from crystal structure data shown by solid), and (b) glass  $\text{Al}_{0.91}\text{La}_{0.09}$ . Term  $2kr_s$  is added to the phase of  $\chi'(k)$ .

resultant  $\chi'(k)$  obtained by combining the data with the cumulant expansion for the  $k$  between 0 and  $3 \text{ \AA}^{-1}$  for the amplitude ratio and between 0 and  $3.5 \text{ \AA}^{-1}$  for the phase difference, is plotted in Fig. 6(a). The cutoff factor  $\sigma_c^2 = 0.015 \text{ \AA}^2$  was used to decrease the Fourier transform  $k_2$  cutoff wiggles by multiplying  $\chi'(k)$  by  $e^{-2k^2\sigma_c^2}$ .

Since the crystal structure is known, a theoretical  $\chi_{\text{th}}(k)$  can be calculated straightforward, assuming that all the 9 paths to Al atoms within the first shell have the same  $B(k)$ , as justified by Fig. 5:

$$\chi_{\text{th}}(k) = B(k) e^{-2k^2\sigma_T^2} \sum_{i=1}^9 N_i \nu_i \frac{e^{i2kr_i}}{r_i^2}, \quad (14)$$

where  $\sigma_T^2 = 0.0027 \text{ \AA}^2$  is a thermal Debye-Waller factor,  $N_i$  is a coordination number of the  $i$  subshell of Al atoms,  $r_i$  is the radius of the  $i$  subshell determined from fit, and fraction coefficient  $\nu_i$  [ $\nu_i = \frac{1}{3}$  for La(1)-Al paths and  $\frac{2}{3}$  for La(2)-Al paths] corrects for different occupancies of La(1) and La(2) atoms in the cell. Dividing  $\chi_{\text{th}}(k)$  by  $\chi_s(k)$  [Eq. (5)] we obtain the theoretical  $\chi'_{\text{th}}(k)$  which contains only structural information. The same  $\sigma_c^2$  was used to decrease the Fourier transform cutoff wiggles at  $k_2$ . Figure 6(a) demonstrates the good agreement between  $\chi'(k)$  and  $\chi'_{\text{th}}(k)$  for the crystal. The  $\sin(2kr)$  transform was performed for both data and theory [Eq. (9)]. The resultant RDF's are shown in Fig. 7(a). The negative values are cutoff wiggles due to the finite value of the upper limit  $k_2$ . We checked this by extending  $k_2$  in

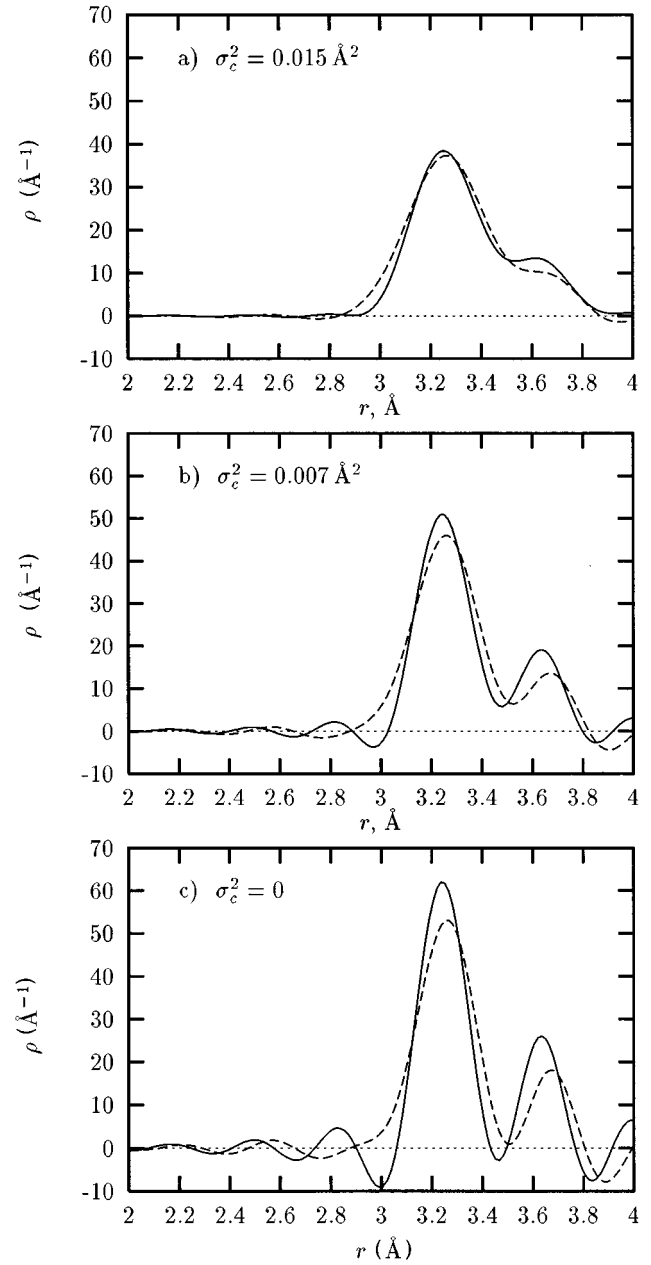


FIG. 7. Radial distribution functions  $\rho(r)$  for the crystal  $\text{Al}_{11}\text{La}_3$  (from XAFS data shown by dash, from crystal structure data shown by solid). The cutoff factor is (a)  $0.015 \text{ \AA}^2$ , (b)  $0.007 \text{ \AA}^2$ , and (c) 0.

Eq. (9) to  $\infty$  for the model structure calculation and the oscillations disappeared. The coordination number, defined as the area below the RDF curve, is equal  $16.0$  from crystallography data and  $16.0 \pm 0.2$  for the XAFS crystal data. The centroid of  $\rho(r)$  is at  $\langle R \rangle = 3.32 \pm 0.30 \text{ \AA}$  for XAFS data and  $3.32 \text{ \AA}$  for diffraction data.

The fine details of the crystal structure, namely nine different Al subshells, are not revealed in Fig. 7(a) because of the spatial resolution  $\delta r = 0.3 \text{ \AA}$ . Such a poor resolution is caused, in accordance with Eq. (11), by the finite value of  $k_2$  and the introduced Gaussian cutoff factor  $\sigma_c^2 = 0.015 \text{ \AA}^2$ .

Changing the cutoff factor gradually from  $0.015 \text{ \AA}^2$  to zero we resolve more and more structure for the crystal data.

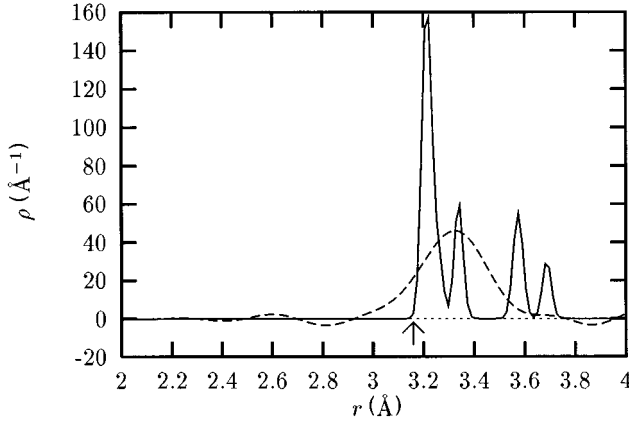


FIG. 8. Radial distribution functions  $\rho(r)$  for the glass  $\text{Al}_{0.91}\text{La}_{0.09}$  (dash) and for crystal  $\text{Al}_{11}\text{La}_3$  using crystallographic data (solid). The cutoff factor  $\sigma_c^2=0$ . Arrow shows the shortest distance to the first-nearest neighbor in the crystal as obtained from diffraction data.

As one can see from comparing the calculated RDF's for the crystal, obtained with different resolutions ( $\sigma_c^2 = 0.015, 0.007, \text{ and } 0 \text{ \AA}^2$ ), the cutoff factor has affected the shape and the width of the distribution  $\rho_{\text{th}}(r)$  dramatically. Figures 7(a)-7(c) demonstrate how the more distant groups of Al atoms form a shoulder on the RDF which becomes resolved as the resolution increases. In demonstrating the splitting into subshells in the calculated RDF and to avoid the cutoff wiggles the  $\chi'(k)$  was calculated to high values in  $k$  space (e.g., up to  $50 \text{ \AA}^{-1}$ ) where no cutoff factor is needed. The required vanishing of  $\chi'(k)$  was provided by the thermal, Debye-Waller factor  $\sigma_T^2$  [Eq. (14)] only. As a result one can see four groups of Al subshells which are associated with four peaks in Fig. 8. The first peak is formed by the five shortest La-Al distances (see Table II), the second is caused by the sixth subshell, the third one corresponds to the group of the next two more distant subshells, and the last peak is formed by the ninth subshell. The spatial resolution here is  $0.01 \text{ \AA}$ . An important consequence of the improvement of the resolution is that the left wing of the peak on the theoretical RDF has become steeper, approaching its crystallographic value  $\approx 3.2 \text{ \AA}$ .

The remarkable agreement between the diffraction data and the XAFS data for the crystal gives us confidence in the accuracy of our procedure as applied to the glass  $\text{Al}_{0.91}\text{La}_{0.09}$ . An assumption was made that the first shell in the glass is populated by Al atoms only as was the case for the crystal. It was confirmed by both the lack of unphysical negative values in the resulting  $\rho(r)$  and Monte Carlo simulations as described below. We used the same Hanning window in  $r$  space to isolate the first shell for the glass as for the crystal [Fig. 4(b)]. Due to the high disorder in the glass structure our initial attempt to fit the first shell by the more standard method of assuming a distribution slightly perturbed from a Gaussian by using only four leading cumulants was unsuccessful: the fit was not good and gave a too high coordination number (22) to be reasonable.

The splice method was much more successful. It assumes that the distribution is seen approximately Gaussian for the low- $k$  electrons only,<sup>5</sup> since the width of the distribution is

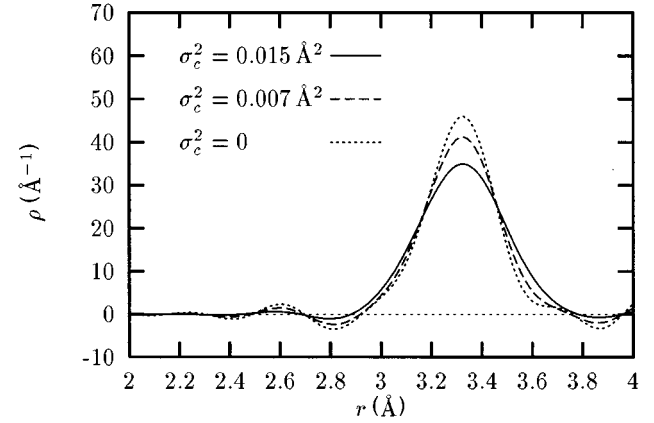


FIG. 9. Radial distribution functions  $\rho(r)$  for the glass  $\text{Al}_{0.91}\text{La}_{0.09}$ . Different curves correspond to cutoff factors  $0.015 \text{ \AA}^2$ ,  $0.007 \text{ \AA}^2$  and  $0$ .

narrow compared to their wavelengths and the spatial resolution [Eq. (11)] is poor. Therefore it is a good approximation to truncate the cumulants expansion at third order for  $k$  below  $k_1$  and use experimental data in the range between  $k_1$  and  $k_2$  where higher-order cumulants are more important. We checked the validity of this approximation later, when  $\rho(r)$  was obtained and cumulants were determined using Eq. (4). It was obtained that the term with  $C_4$  in the cumulant expansion [Eq. (3)] with  $k=3 \text{ \AA}^{-1}$  is only 10% of the term with  $C_2$ , thus justifying the approximation used. The whole method therefore is self-consistent, since we use the cumulant expansion in the range where it converges rapidly, and the experimental data where it does not.

The glass data  $\chi_{\text{gl}}(k)$  (Fig. 2) was transformed in the same way as the crystal data and the theoretical calculation above, using the same  $k_2$  and  $\sigma_c^2$ . The cumulants needed to extrapolate  $\chi'_{\text{gl}}(k)$  between  $k=0$  and  $3.0 \text{ \AA}^{-1}$  (for the amplitudes ratio) and between  $k=0$  and  $3.5 \text{ \AA}^{-1}$  (for the phase difference) were obtained. The ratio  $\chi'(k)$  obtained by splicing the data with the cumulant expansion for the  $k$  between 0 and  $3 \text{ \AA}^{-1}$  for the amplitude ratio and between 0 and  $3.5 \text{ \AA}^{-1}$  for the phase difference, is plotted in Fig. 6(b). To study how the cutoff factor  $\sigma_c^2$  affects the RDF of the glass we have varied  $\sigma_c^2$  from  $0.015 \text{ \AA}^2$  to 0 (as it was done above for the crystal) and compared the resultant RDF's. The resultant  $\rho(r)$  obtained with the same cutoff factors as used for the crystal are shown in Fig. 9. It turns out that, contrary to the crystal, the glassy RDF's look similar and little change in the broadening occurred (Fig. 9), indicating that the  $\rho(r)$  of the glass has inherent broadening which is not introduced by the cutoff factor.

Calculations of coordination number and the average La-Al distance over the shell give the following results:  $N = 14.45 \pm 0.10$ ,  $\langle R_{\text{La-Al}} \rangle = 3.33 \pm 0.05 \text{ \AA}$ . Comparing the two RDF's for the glass and the crystal (Fig. 8) we conclude that the distribution of atoms in the glass has some shorter bonds than the crystalline structure allows, as it was previously found in Monte Carlo simulations.<sup>15</sup> The number of Al atoms-nearest neighbors to La is found by evaluation of the area under the glass RDF within the distances from 0 to  $3.16 \text{ \AA}$  (the distance to the left edge of the RDF for crystal, Fig.

TABLE III. First four cumulants found using the ratio and splice methods for the crystal and the glass XAFS data.

	Method	$C_0$	$C_1$ (Å)	$C_2$ (Å <sup>2</sup> )	$C_3$ (Å <sup>3</sup> )
Crystal	Ratio	2.28(3)	-0.09(1)	0.0011(3)	0.0014(2)
Crystal	Splice	2.77(2)	-0.02(1)	0.0170(10)	0.0031(3)
Glass	Ratio	2.40(8)	-0.01(1)	0.0098(9)	0.0009(1)
Glass	Splice	2.67(1)	-0.01(1)	0.0100(2)	0.0021(4)

8). The result is  $N = 1.7 \pm 0.1$  which means that that number of shorter bonds occur in the glass. The mean of these short bond lengths is  $3.09 \pm 0.05$  Å.

As it was discussed by Stern *et al.*,<sup>5</sup> the absence of the experimental data below  $k_1$  makes it in principle impossible to reconstruct large variations, of  $|\chi'(k)|$  which may occur and be confined between 0 and  $k_1$ . These variations, if they exist, would give rise to a broad distribution  $\rho_b(r)$  which we are unable to detect since the extrapolation with cumulants to  $k=0$  does not carry information about  $\rho_b(r)$ . We, however, are able to estimate the minimum width  $\sigma_b$  of this distribution, assuming for simplicity that it is Gaussian. If the error introduced by neglecting the contribution of  $\rho_b(r)$  to  $\rho(r)$  (which we determined by the splice method) is as big as 10%, i.e.,  $\exp(-2k_1^2\sigma_b^2) \approx 0.1$ , then  $\sigma_b \approx 0.3$  Å, much greater than the standard deviation of  $\rho(r)$ ,  $\sigma = \sqrt{C_2} \approx 0.1$  Å (Table III). It means that, if present,  $\rho_b(r)$  would be a relatively broad background to  $\rho(r)$  which does not affect its shape significantly. As to the coordination number, it would be affected by adding such a background to  $\rho(r)$ , but since we expect the correction to the coordination number to be small, the background must be small too.

## V. MONTE CARLO SIMULATION

Monte Carlo simulations were performed to analyze the glassification mechanism in Al-La alloy. The system consisted of 1000 atoms of Al and La in the ratio 9:1. Initially all atoms were placed in a cubic cell. The size of the cubic cell was chosen in such a way that the density of the glass corresponds to its experimentally known value.<sup>16</sup> To describe the interaction between pairs of atoms the Lennard-Jones potential  $U_{\alpha\beta} = B_{\alpha\beta}r^{-12} - A_{\alpha\beta}r^{-6}$  was used. This potential showed good agreement with experiment for other systems, e.g.,  $\text{Ni}_x\text{P}_{1-x}$ ,<sup>17</sup>  $\text{Zn}_x\text{Mg}_{1-x}$ , and  $\text{Zr}_x\text{Cu}_{1-x}$ .<sup>18</sup>

The parameters  $A_{\text{Al-Al}}$ ,  $A_{\text{La-La}}$ , and  $A_{\text{Al-La}}$  describe the dipole-dipole interaction between pairs of atoms. To calculate these parameters we used the known atomic radii and valences of pure Al and La (Ref. 19) and followed the standard procedure described in Ref. 15. Parameters  $B_{\text{Al-Al}}$  and  $B_{\text{La-La}}$  were chosen from the Monte Carlo simulation for pure Al and La in such a way that the first peaks of the radial distribution functions and densities corresponded to their respective values in the crystalline phases. To define  $B_{\text{Al-La}}$  our XAFS result for the average La-Al nearest-neighbor distance (3.3 Å) was used. Periodic boundary conditions were imposed. The above-mentioned input parameters, taken alone, do not lead to a unique atomic arrangement without specifying the relevant relaxation procedure. We followed the Metropolis procedure to obtain the relaxed system, which

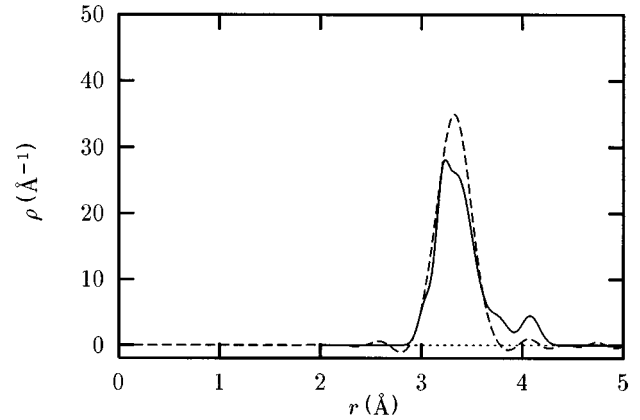


FIG. 10. Radial distribution functions for the glass  $\text{Al}_{0.91}\text{La}_{0.09}$  obtained with the splice method of XAFS (dash) and Monte Carlo simulations (solid).

corresponded to the glassy state. To evaluate the necessary relaxation time for the determination of the required number of Monte Carlo steps an additional estimation of the diffusion coefficient was performed. The number of steps was chosen to be sufficient for the randomly diffusing atom to pass the distance between two opposite walls.

The simulation results are in qualitative agreement with our XAFS results as shown in Fig. 10. The  $\rho(r)$  found from the simulations is similar to the experimental result from XAFS even though the Lennard-Jones potential may be an oversimplified approximation. First, the La atoms are separated from each other by distances larger than  $4.1 \pm 0.1$  Å, confirming our assumption above that the first coordination shell in the glass within 2.0–4.0 Å around the La is populated by Al atoms only. Second, the coordination number 14.5 is obtained by averaging over all La atomic environments, agreeing with the XAFS result ( $14.45 \pm 0.10$ ). Similar bond shortening to that found from XAFS was found in our simulations, including a shortest La-Al distance of  $3.0 \pm 0.1$  Å.

## VI. DISCUSSION

The splice method was a powerful method to determine the distribution in this case for both the glass and the crystal since it did not have to assume a small deviation from a Gaussian distribution. As was shown, assuming the first few terms of the cumulant expansion to be sufficient to describe the distribution throughout the full  $k$  range is not valid unless the deviation from a Gaussian is small for all values of  $k$ . When such is not the case, then the expansion by a finite series of cumulants becomes possible only for the low- $k$  portion of the data, and assuming that this is true for the full range introduces errors. In our case this assumption underestimates the deviations of the true  $\rho(r)$  from the Gaussian. Table III shows the difference between the cumulants found with the ratio method for the full  $k$  range and the final results, using power moments of  $g(r)$  [Eq. (4)] for the crystal and glass data. Second cumulants obtained by the splice method (Table III) do not contain the cutoff factor  $\sigma_c^2$ , added previously to  $\chi'(k)$ , which was subtracted later to compare them with  $C_2$  obtained by the ratio method. The

rest of the cumulants are not affected by this Gaussian factor. The importance of defining the  $E_0$  to be the muffin-tin zero level was also emphasized. The only reliable method to determine  $g(r)$  is the splice method. It combines the  $\chi'(k)$  defined within the whole data  $k$  range with its cumulant expansion at low  $k$ .

The coordination number and La-Al distance agree well with  $\text{Al}_{0.9}\text{Y}_{0.1}$  metallic glass determined by anomalous x-ray scattering<sup>1</sup> where  $N = 14.2 \pm 1.3$  and  $\langle R_{\text{Y-Al}} \rangle = 3.2 \text{ \AA}$ . The similarity in structures of  $\text{Al}_{0.91}\text{La}_{0.09}$  and  $\text{Al}_{0.9}\text{Y}_{0.1}$  is expected since La and Y have almost the same concentration in their glasses, and their atomic radii are rather close: La radius is  $1.88 \text{ \AA}$  and Y radius is  $1.80 \text{ \AA}$  at room temperature.<sup>20</sup>

The accuracy of the analysis of the amorphous and crystalline phases by the splice method was clearly demonstrated by comparing with diffraction data of the crystal. The results obtained for the first shell of La atoms show that the mean first-nearest-neighbor La-Al distances in the glass and crystal are close to each other within uncertainties. However, while the coordination number for the glass was found to be  $N_g = 14.45 \pm 0.10$ , the crystalline phase is characterized by a larger coordination number:  $N_c = 16$ . The RDF's of these two samples are quite different: Figs. 7 and 9 demonstrate that the RDF of  $\text{Al}_{11}\text{La}_3$  has a structure within about  $3.5\text{--}3.8 \text{ \AA}$  around the central La, associated with more distant shells of the Al atoms, while the RDF of the glass  $\text{Al}_{0.91}\text{La}_{0.09}$  looks more compact and symmetric.

It has been generally recognized that the glass-forming range of composition for binary metallic glasses is an approximate universal property of atomic size ratio of the constituent elements.<sup>21,22</sup> In the case of the *smaller* foreign atoms  $A$  being incorporated into the *larger* host atoms  $B$ , the glass forming ability is enhanced with their size difference increase. The composition range for the glass formation is related directly to the compositional dependence of the melting point of the alloy,  $T_m$ . This is because the glass transition temperature  $T_g$  is almost independent of composition, while the melting temperature usually decreases to a minimum near 50% composition. In the ranges of composition where  $T_m$  is closer to  $T_g$ , the glass formation is easier. The deep depressions of the liquidus curve usually occur when the sizes of the constituent atoms differ dramatically, and thus the glass formation is generally more favorable to alloys with large size difference of the constituent elements. As a criterion for minimum solute concentration  $C_A^{\text{min}}$  for glass formation and the atomic radii ratio  $r_A/r_B$  the empirical relationship<sup>22</sup> is often used:

$$C_A^{\text{min}} \left| 1 - \frac{r_A}{r_B} \right| \approx 0.1. \quad (15)$$

In the case of the *larger* foreign atoms  $A$  being incorporated into the *smaller* host atoms  $B$ , as in our case, where  $A = \text{La}$ ,  $B = \text{Al}$ , another important factor to form a glassy phase comes into consideration. Experimental data on phase diagrams of different binary metallic alloys<sup>23</sup> in thermal equilibrium (see, e.g., In-Ga, K-Na, Na-Rb) show that the range of concentration where  $A$  dissolves in  $B$  is smaller than where  $B$  dissolves in  $A$ . This introduces a tendency to make the alloy of large atoms in a smaller atom host less stable than vice versa. The glass formation in the alloy with low concentration of large atoms in small host atoms would become less likely because the alloy would have a greater tendency to separate before the glass transition occurs. It is shown here that there is a significant fraction of La-Al atomic bonds in the glass that are shorter than in the crystal. This bond shortening decreases the radii ratio, making the glassification of La-Al alloy more favorable under rapid quench.

## VII. SUMMARY AND CONCLUSIONS

XAFS measurements and analysis of metallic glass  $\text{Al}_{0.91}\text{La}_{0.09}$  and the crystalline phase  $\text{Al}_{11}\text{La}_3$ , obtained after annealing the glass, were performed. The XAFS data were analyzed by the splice method. The advantage of the splice method over cumulant expansion fitting and ratio methods was demonstrated and discussed. The calculations of the radial distribution function and cumulants were performed using the program RDF and the UWXAFS data analysis package.<sup>14</sup> The reliability of the method was checked against the known crystal structure and excellent agreement with the RDF reconstructed from the diffraction data for this structure was obtained.

We found a large change in  $\rho(r)$  between the glass and the crystal. The glass exhibits a broad radial distribution of the first-nearest neighbors around La atoms, resulting in some fraction of bonds being shorter than those found in the crystalline phase. This shortening decreases the size disparity between La and Al atoms, explaining the glass formation at unusually low concentration of La. We suggest this as a general scenario which has not been considered previously for a wide class of amorphous alloys.

## ACKNOWLEDGMENTS

Authors are grateful to V. Manov for his help in the sample preparation and to Yu. Rosenberg for performing x-ray-diffraction measurements. This work was supported by the US-Israel BSF Grant No. 90-00152/1 and in part by DOE Grant No. DE-FG06-90ER45425. Beamline X11A is supported by DOE Grant No. DE-FG05-89ER45384. Simulations were supported by GIF Grant No. I-140-125.7/89.

<sup>1</sup>A. Inoue, K. Ohtera, and T. Masumoto, Sci. Rep. Res. Inst. Tohoku Univ. Ser. A **35**, 115 (1990).

<sup>2</sup>V. Manov, A. Rubshtein, A. Voronel, P. Popel, and A. Vereshagin, Mater. Sci. Eng. **A179/A180**, 91 (1994).

<sup>3</sup>R. W. Cahn, Angew. Chem. **101**, 124 (1989).

<sup>4</sup>A. Rubshtein, Yu. Rosenberg, A. Frenkel, V. Manov, E.

Veliyulin, A. Voronel, and E. A. Stern, Mater. Sci. Forum **179-181**, 839 (1995).

<sup>5</sup>C. E. Bouldin, Ph.D. thesis, University of Washington, 1984; Y. Ma and E. A. Stern, Physica B **158**, 268 (1989); E. A. Stern, Y. Ma, O. Hanske-Petitpierre, and C. E. Bouldin, Phys. Rev. B **46**, 687 (1992).

- <sup>6</sup>E. A. Stern, D. E. Sayers, and F. W. Lytle, *Phys. Rev. B* **11**, 4836 (1975).
- <sup>7</sup>E. A. Stern and S. M. Heald, in *Handbook on Synchrotron Radiation*, edited by E. E. Koch (North-Holland, Amsterdam, 1983), Chap. 10.
- <sup>8</sup>E. D. Crozier, J. J. Rehr, and R. Ingalls, in *X-ray Absorption: Principles, Applications of EXAFS, SEXAFS and XANES*, edited by D. C. Koningsberger and R. Prins (Wiley, New York, 1988), Chap. 9.
- <sup>9</sup>G. Bunker, *Nucl. Instrum. Methods Phys. Res.* **207**, 437 (1983).
- <sup>10</sup>E. A. Stern and K. Kim, *Phys. Rev. B* **23**, 3781 (1981).
- <sup>11</sup>M. Newville, P. Livins, Y. Yacoby, J. J. Rehr, and E. A. Stern, *Phys. Rev. B* **47**, 14 126 (1993).
- <sup>12</sup>J. J. Rehr, R. C. Albers, and S. I. Zabinsky, *Phys. Rev. Lett.* **69**, 3397 (1992); J. Mustre de Leon, J. J. Rehr, S. I. Zabinsky, and R. C. Albers, *Phys. Rev. B* **44**, 4146 (1991).
- <sup>13</sup>A. H. Gomes de Mesquita and K. H. J. Buschow, *Acta Crystallogr.* **22**, 497 (1967).
- <sup>14</sup>E. A. Stern, M. Newville, B. Ravel, Y. Yacoby, and D. Haskel, *Physica B* **208 & 209**, 117 (1995).
- <sup>15</sup>Y. Ben Ezra and V. Fleurov, *Solid State Commun.*, **89**, 591 (1994).
- <sup>16</sup>O. Gorodetsky (private communication).
- <sup>17</sup>W. Y. Ching, *Phys. Rev. B* **34**, 2080 (1986).
- <sup>18</sup>W. Y. Ching, G.-L. Zhao, and Y. He, *Phys. Rev. B* **42**, 10 878 (1990).
- <sup>19</sup>T. Egami and Y. Waseda, *J. Non-Cryst. Solids* **64**, 113 (1984).
- <sup>20</sup>*Handbook of Chemistry and Physics*, edited by R. C. Weast (CRC, Boca Raton, Florida, 1974), p. B-233.
- <sup>21</sup>A. L. Greer, *Science* **267**, 1947 (1995).
- <sup>22</sup>T. Egami and S. Aur, *J. Non-Cryst. Solids* **89**, 60 (1987).
- <sup>23</sup>M. Hansen and K. Anderko, *Constitution of Binary Alloys*, 2nd ed. (McGraw-Hill, New York, 1958).